PROCEEDINGS OF SCIENCE

Study of the Scattering of the halo nucleus ^{11}Be on a ^{197}Au target at energies around the Coulomb barrier

M.J.G. Borge[*†], **V. Pesudo**[‡], **E. Nácher, O. Tengblad, M. Cubero, A. Perea**
Instituto de Estructura de la Materia, CSIC, 28006 Madrid, Spain
mgb@cern.ch

A.M. Moro, J.A. Lay, J. Gómez-Camacho, M.A.G. Alvarez, J.P. Fernández-García
Departamento de FAMN, Universidad de Sevilla, 41080 Sevilla, Spain

A. Di Prieto, P. P. Figuera, M. Fisichella, M. Lattuada, V. Scuderi
Laboratori Nazionali del Sud, INFN, via Santa Sofia 62, 95123, Catania, Italy

G. Marquínez-Durán, I. Martel, A.M. Sánchez-Benítez
Departamento de Ciencias integradas, Universidad de Huelva, 21071 Huelva, Spain

M. Alcorta, P. C. Bender, R. Braid, A.B. Garnsworthy, G. Hackman, D. Miller, M. Moukaddam, M.M. Rajabali, C. Unsworth, Z.M. Wang
TRIUMF, 4004 Wesbrook Mall, Vancouver, British Columbia V6T 2A3, Canada

B.R. Fulton
Department of Physics, University of York, YO 10 5DD Heslington, York, UK

U. Hager
National Superconducting Cyclotron Laboratory, Michigan State University, East Lansing, MI 48824, USA

O.S. Kirsebom
Department of Physics and Astronomy, Aarhus University, 8000 Aarhus, Denmark

K. Kuhn, P.D. O'Malley, F. Sarazin
Physics Department, Colorado School of Mines, Golden, Colorado 80401, USA

C.E. Svensson
Dept. of Physics. University of Guelph, Guelph, Ontario N1G 2W1, Canada

PoS(INPC2016)207

The angular distributions of the elastic, inelastic scattering and break-up cross sections of the one neutron halo ^{11}Be on a heavy-mass target (^{197}Au) have been measured at laboratory energies below (31.9 MeV) and around (39.6 MeV) the Coulomb barrier ($V_b \sim 40$ MeV). The elastic, inelastic channel and break-up channels of the ^{11}Be + ^{197}Au reaction have been experimentally separated for the first time in this energy range. The experiment was performed at TRIUMF, using four Silicon detectors in telescope configuration to separate the ^{11}Be from the ^{10}Be fragments and the High-Purity Germanium Detector Array TIGRESS for γ-ray detection. The break-up and inelastic scattering contributions are observed to be relevant even at energies well below the Coulomb barrier. Data are compared with different models of increasing degree of sophistication: semiclassical, inert-core continuum discretised coupled channel (CDCC) calculations and CDCC including core deformation and excitations (XCDCC). XCDCC calculations are necessary to reproduce simultaneously elastic, inelastic and break-up scattering data. The results show that the reaction mechanism is sensible to the entanglement of core and halo degrees of freedom in ^{197}Au.

PACS: 25.45.De, 25.70.-z, 27.20.+n

The 26th International Nuclear Physics Conference
11-16 September, 2016
Adelaide, Australia

---

*Speaker.

†Present address: ISOLDE-EP, CERN, CH-1211 Geneva 23, Switzerland.

‡Department of Physics, University of the Western Cape, P/B X17, Bellville ZA-7535, and Themba LABS, Somerset West 7129, South Africa.

1. Introduction

With the advent of the first accelerated radioactive beams a new nuclear structure was discovered. Thirty years ago, Hansen and Jonson [1] interpreted the large interaction cross section observed in ^{11}Li and ^{11}Be by Tanihata [2] as due to an extended neutron distribution, the halo structure.

The halo structure is a threshold phenomenon due to the low binding energy of the last nucleons. The structure developes when one or two weakly-bound nucleons are dominantly in an *s*-shell (or *p*-shell in some rare cases) above a closed-shell core. Due to the weak attraction and the low centrifugal barrier, the wavefunctions of these nucleons have a tail that extends to large radii. In addition, the halo nuclei have other features in common: a reduced core participation in the scattering process and very few bound excited states, if any.

The discovery of halo nuclei has brought renewed interest in the modelling of nuclear reactions. The halo structure will affect the reaction properties at near Coulomb barrier energies. The dynamics of weakly bound nuclei at energies close to the Coulomb barrier are of great interest due to the interplay between the reaction process and the structure of the projectile. A low energies the Coulomb interaction dominates the reaction process with heavy targets, and the low binding energy and the strong dipolar polarizability contribute to a significant enhancement of the break-up cross section, even below the Coulomb barrier.

Current approaches to reaction theory involve different approximations whose validity needs to be checked when applied to exotic nuclei. Our purpose was to study the reaction mechanism of halo nuclei on the strong Coulomb field of the target at energies around the Coulomb barrier. The structure property that will be most relevant in a Coulomb dominated collision is the $B(E1)$ distribution coupling the ground state to other bound states (if any) or to the continuum.

We have explored the scattering of ^{6}He and ^{11}Li in previous experiments [3, 4, 5, 6, 7]. These nuclei do not have any bound excited state, so the observables at hand in inclusive studies are elastic scattering and break-up, for which the scattering angle and energy of the core (^{4}He and ^{9}Li, respectively) fragments were determined. In the ^{11}Li study [6, 7] we found that there is a close relation between the $B(E1)$ distribution and the break-up cross section at forward angles, where the process is dominated by Coulomb break-up. This fact opened the possibility of determining $B(E1)$ distributions for exotic halo nuclei just from the angular distribution of the inclusive break-up cross section. However, the resulting $B(E1)$ distribution had significant discrepancies with those obtained from previous Coulomb break-up measurements [8] at intermediate energies. To investigate further this discrepancy we have considered the case of the one neutron halo ^{11}Be that has the advantage of being a simpler case to model than the two neutron halo nuclei.

The spin-parity of ^{11}Be ground state ($j^{\pi} = 1/2^{+}$) indicates an inversion between the $1p_{1/2}$ and the $2s_{1/2}$ neutron orbits [9] in a simplified single-particle picture, resulting in a $|^{10}\mathrm{Be}\ (0^{+}) \otimes \nu(s_{1/2})\rangle_{1/2^{+}}$ configuration. This configuration, together with the low binding energy (S_n = 0.504 keV), induce the halo. The $1/2^{-}$ excited state ($|^{10}\mathrm{Be}\ (0^{+}) \otimes \nu(p_{1/2})\rangle_{1/2^{-}}$) is located at E_x = 320 keV and is populated through the strongest measured $B(E1)$ transition probability, $B(E1; 1/2^{+} \rightarrow 1/2^{-})$ = 0.116(12) e^{2}fm^2, between bound states [10]. Recently, a new value has been extracted from Coulomb excitation measurements corroborating the previous $B(E1)$ result although giving a value 10% lower [11]. The ground state can also couple to the $J^{\pi} = 1/2^{-}$ and $J^{\pi} = 3/2^{-}$ continuum states

with a $B(E1)$ distribution that has been determined by different methods, showing the same shape of the $B(E1)$ distribution but very different absolute values [12, 13, 14].

Therefore we decided to measure accurately elastic, inelastic and break-up cross sections for ^{11}Be on a high-Z target at energies near the Coulomb barrier and to calculate consistently elastic, inelastic and break-up cross sections, taking into account all continuum excitations in a strongly-coupled Coulomb-dominated situation with the aim of obtaining results consistent with the measured experimental data.

In this contribution we will show the relative distribution for the three channels: elastic, inelastic and break-up and the comparison to different models with higher and higher degree of sophistication.

2. Experimental Setup

The radioactive ^{11}Be beam was produced by the ISOL method in the TRIUMF-ISAC-I (Isotope Separator and ACcelerator), where the 500 MeV 100 μA proton beam from the cyclotron hits a primary tantallum target. Due to the impact of the incoming protons on this thick target ($\sim$20 g/cm^2) a variety of nuclei were produced. The cocktail of products was diffused towards the transfer line where the three laser beams from TRILIS enhance the ^{11}Be ionization efficiency over other species. The beam was cleaned further from contaminants in the mass separator. Then the ^{11}Be beam was sent to an ECR source where it was ionised to a higher mass over charge ratio (A/q) for optimal acceleration in the ISAC-II superconducting Linac to the requested energy of 2.9 MeV/u and 3.6 MeV/u. The intensity of the ^{11}Be beam delivered to our chamber was in average 10^5 pps. The accelerated ^{11}Be beam impinged on a 1.9 mg/cm^2 thick ^{197}Au target tilted 15° with respect to the beam direction. The thickness of this secondary target was chosen as a compromise between statistics and resolution due to the straggling in the target.

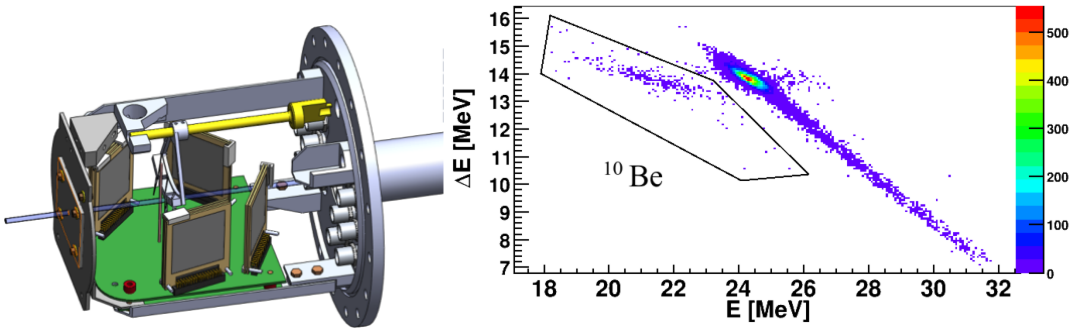

Figure 1: On the left hand side a 3D-drawing showing the chamber hosting the four telescopes positioned in a printed circuit board. On the right hand side, a two-dimensional spectrum of the ^{11}Be +^{197}Au reaction at E_{lab} = 39.6 MeV for a pixel at 18°. The energy lost in the ΔE detector is represented in the Y axis, versus energy deposited in the back detector in the X axis. The locus with more statistics corresponds to the quasi-elastically scattered ^{11}Be beam. The other locus corresponds to the ^{10}Be fragments detected after break-up as indicated.

The setup for the detection of charged particles consisted of four telescopes (T1-T4) which were positioned as given in Table 1. The solid angle covered by the setup ranges from 14° to 157°.

Telescope	Central Polar Angle	Angular range	Dist. (mm)
T1	28°	14°-43°	80
T2	45°	23°-68°	60
T3	76°	55°-97°	60
T4	120°	102°-157°	50

Table 1: Polar angle at which the Silicon detectors are placed with respect to the beam direction and distance of the front detector of the telescope to the center of the target.

The difference distances of the telescopes to the target try to compensate from the losses of counts at backward angles. The asymmetric distribution of the telescopes as well as the inclination of the target are optimised to have overlap in the angular range covered by the telescopes and reduce the shadowing of the target frame. The layout of the telescopes setup is shown on the left hand side of Fig. 1 The T1-T3 telescopes consisted of a 40 μm thick double-sided silicon strip detector (DSSSD) acting as a ΔE detector backed with a 500 μm Si PAD able to stop the ions completely. T4 had a 20 μm single-sided silicon strip detector (SSSSD) as ΔE and a 300 μm DSSSD as an E-detector. A thinner ΔE was chosen to ensure that ions emitted at backward angles passed through it. It should be noticed that there was one DSSSD in each of the telescopes allowing for high granularity in the full angular range.

The coincidence between the vertical and horizontal strips results in 3×3 mm^2 pixels (each pixel subtends angles around 3°), giving a high angular resolution. The telescopes were cabled and positioned using a printed circuit board (PCB). For the data analysis the angle and position of the telescopes was determined for the first three telescope by fitting the elastic scattering of 5.04 MeV/u ^{12}C beam on ^{197}Au to the Rutherford angular distribution.

The experimental setup was surrounded by two of the three TIGRESS rings for gamma detection [15], the ring at θ_{lab} = 90° consisted of eight clovers and the one at 135° of four clovers, the HPGe detectors were uniformly distributed in the ring. The total gamma efficiency was 12.8 % at 320 keV, the energy of the γ-ray connecting the only bound excited state in ^{11}Be to its g.s. The 320 keV γ-ray was well separated from the 268.8 and 279.0 keV γ-rays from de-excitation of states in ^{197}Au. Due to the Doppler broadening of the γ-rays coming from the excitation with the beam, they were easily distinguishable from those of the excitation of the target. In addition the energy resolution of TIGRESS after doppler correction was found in this experiment to be 7 keV at the relevant energies. The γ-ray in coincidences with charged particles were used to obtain the contribution of the inelastic channel.

The strips of the DSSSD were energy calibrated using two radioactive sources, ^{148}Gd and the triple-α source (^{239}Pu + ^{241}Am + ^{244}Cm). In order to separate well the signals from heavy ions and avoid beta contributions, a condition was set to validate the events: the difference between the energy deposited in the front and back strip of the same DSSSD forming the pixel should be less than 200 keV.

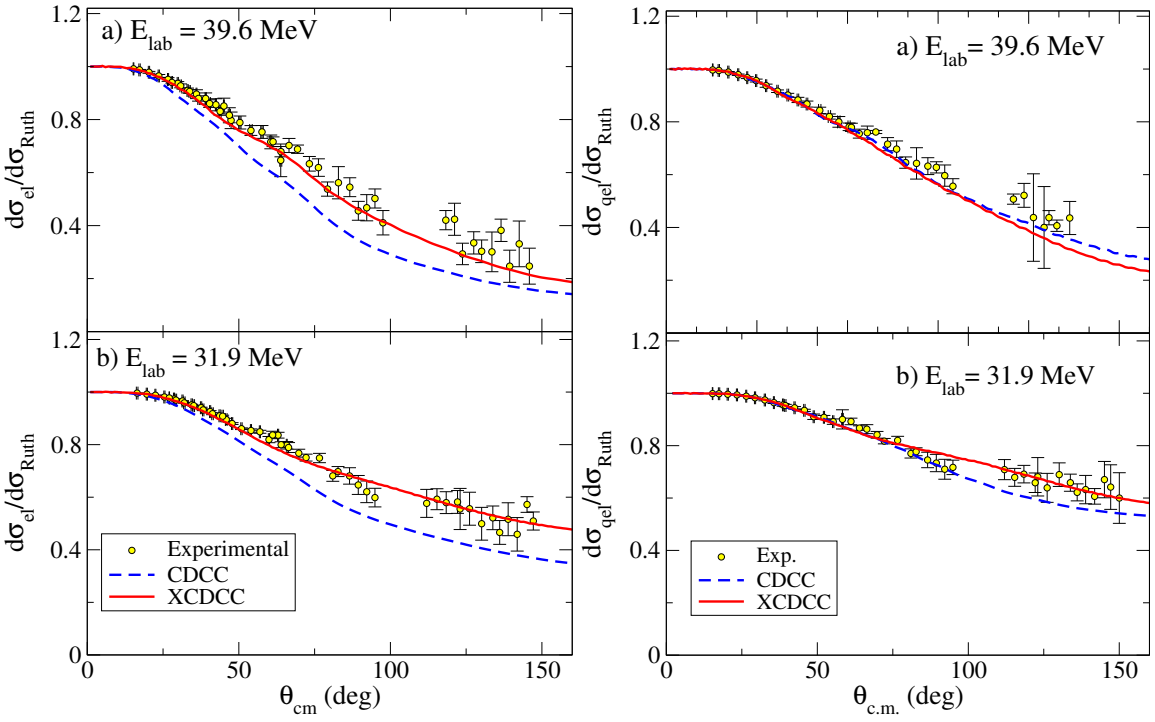

Figure 2: On the left hand side the measured differential elastic scattering cross section of ^{11}Be + ^{197}Au at $E_{c.m.} = 37.1$ MeV (top) and $E_{c.m.} = 29.6$ MeV (bottom) relative to Rutherford is compared with the CDCC and the XCDCC calculations. There is a significant deviation of the scattering data from the Rutherford formula in the full angular range, even where Coulomb interaction dominates, showing the importance of the dipole polarizability in the collision process. The CDCC calculations underestimates the elastic data since the coupling to the bound excited state in this model is too strong, as discussed in the text. On the right hand side the differential quasielastic cross section relative to Rutherford is shown for ^{11}Be + ^{197}Au at $E_{c.m.} = 37.1$ MeV (top) and $E_{c.m.} = 29.6$ MeV (bottom). One can see that the CDCC model describes rather well the quasielastic data. XCDCC accounts well for the differential elastic and quasielastic scattering data in the full angular range.

3. Analysis and Results

We were interested in measuring the ^{11}Be + ^{197}Au reaction at energies below and around the Coulomb barrier, estimated to be around 40 MeV. Therefore the reaction was studied at energies of the incoming ^{11}Be beam of 31.9 and 39.6 MeV.

The ^{11}Be + ^{197}Au data were first analysed assuming that the forward detectors were at the position determined by the geometrical measurements, and the optical beam axis centred in the ^{197}Au target. Due to the close geometry of the setup, a refined determination of the angle subtended by each pixel of the telescope was done based on the fact that the elastic scattering of ^{12}C + ^{197}Au at energies below the barrier should follow the Rutherford formula. The method could only be applied to the T1-T3 telescopes. The angles covered by the pixel of the T4 telescope were determined only by geometrical considerations as the angular dependence of the cross section is less steep. The differential cross section with optimised position vectors for each pixel was divided by the solid angle of the pixel. The differential cross sections were obtained by summing contributions of

the different pixels within a certain angular range and divided by the solid angles of the pixels included in the same angular range. Figure 1 illustrates an example of the raw data from T1 telescope obtained for the 39.6 MeV ^{11}Be beam scattered on the ^{197}Au target at 18°. The two-dimensional plots for the ^{11}Be scattered data show the contribution of the quasielastic (elastic + inelastic) channel and the ^{10}Be break-up one. It is noticeable that the break-up channel is large even at very forward angles. A clear separation of the quasielastic and break-up data is achieved. By requiring coincidences with the 320 keV γ-ray and removing background contributions the inelastic contribution was separated from the elastic one.

The measured angular distributions are compared with different calculation of increasing complexity, first the traditional optical model for which a effective potential describing the elastic scattering is derived, for more details see [17]. Then a first-order semiclassical calculation including $E1$ couplings, known as the equivalent photon method (EPM) [18]; a continuum-discretized coupled channels (CDCC) calculation, including bound and unbound states of the n + ^{10}Be system and couplings among them to all orders; and an extended CDCC calculation (XCDCC) [24, 25] which incorporates the entanglement of the ^{10}Be core states, the 0^+ ground state and the first 2^+ state, with the single particle states of the valence neutron.

The comparison with the data is shown in Figs. 2 and 3. A brief description of the models used and their comparison to the data are given in the following.

In the EPM calculations, the projectile is considered to follow a classical Coulomb trajectory and the excitation cross section is given as the probability, for a given trajectory, of populating an excited state. The excitation process is, thus, treated perturbatively and does not alter the trajectory. The EPM calculation shown here includes only first order effects.

The CDCC calculation includes bound and unbound states of the n + ^{10}Be system and couplings among them to all orders. The traditional CDCC formalism describes the projectile states within a single-particle model (SP) that ignores the structure of the ^{10}Be core and describes the motion of the halo using a mean-field potential of Wood-Saxon type. In the CDCC calculations, the reaction is modelled as an effective three-body problem (^{10}Be + n + ^{197}Au) and break-up is treated as excitations of the ^{11}Be nucleus to ^{10}Be + n continuum states, which are conveniently discretized using a binning procedure. For the ^{10}Be + n interaction, we used the SP model of Capel et al. [21]. This potential reproduces the separation energy of the ground and first excited state of the ^{11}Be nucleus (assuming pure $2s_{1/2}$ and $1p_{1/2}$ configurations for these states, respectively) and predicts a $B(E1)$ distribution to the continuum in good agreement with the experimental distribution from Ref. [14]. For the ^{10}Be + ^{197}Au potential, we used the optical model fit reported in Ref. [19] for the ^{10}Be + ^{208}Pb reaction at a similar energy to that used here (with the radius scaled to account for the mass difference of the target) and the n+^{197}Au potential was obtained from the local parametrization of Koning and Delaroche [20].

The XCDCC describes the dynamic of the process as the CDCC improving in the description of the projectile, i.e. uses the particle-rotor model, whose potential parameters are taken from [22]. The interaction of the halo neutron with the core has a quadrupole deformation of $\beta = 0.67$ [23]. In particular, the ^{11}Be ground state is considered as a linear combination of $|^{10}\mathrm{Be(gs)}\times\nu(2\mathrm{s}_{1/2})\rangle$, $|^{10}\mathrm{Be}(2^+)\times\nu 1\mathrm{d}_{5/2}\rangle$ and $|^{10}\mathrm{Be(gs)}\times\nu(1\mathrm{d}_{3/2})\rangle$, where the dominant component at the level of 80% is the one involving the ^{10}Be(gs). Excitations of the ^{10}Be core are included in the so called XCDCC calculation [24, 25] where contributions of the ^{10}Be first excited state (2^+, E_{exc} = 3.37 MeV) are

Model	Reaction (mb)	Inelastic (mb)	Break-up (mb)	Absoption (mb)
		E_{lab} = 31.9 MeV		
CDCC	6735	3894	2279	562
XCDCC	4394	1905	1971	518
		E_{lab} = 39.6 MeV		
CDCC	7640	4212	2592	836
XCDCC	5602	1966	2409	1227

Table 2: Calculated angle-integrated cross sections: inelastic, break-up and absorption, which includes other channels such as complete or incomplete fusion within the CDCC and XCDCC framework.

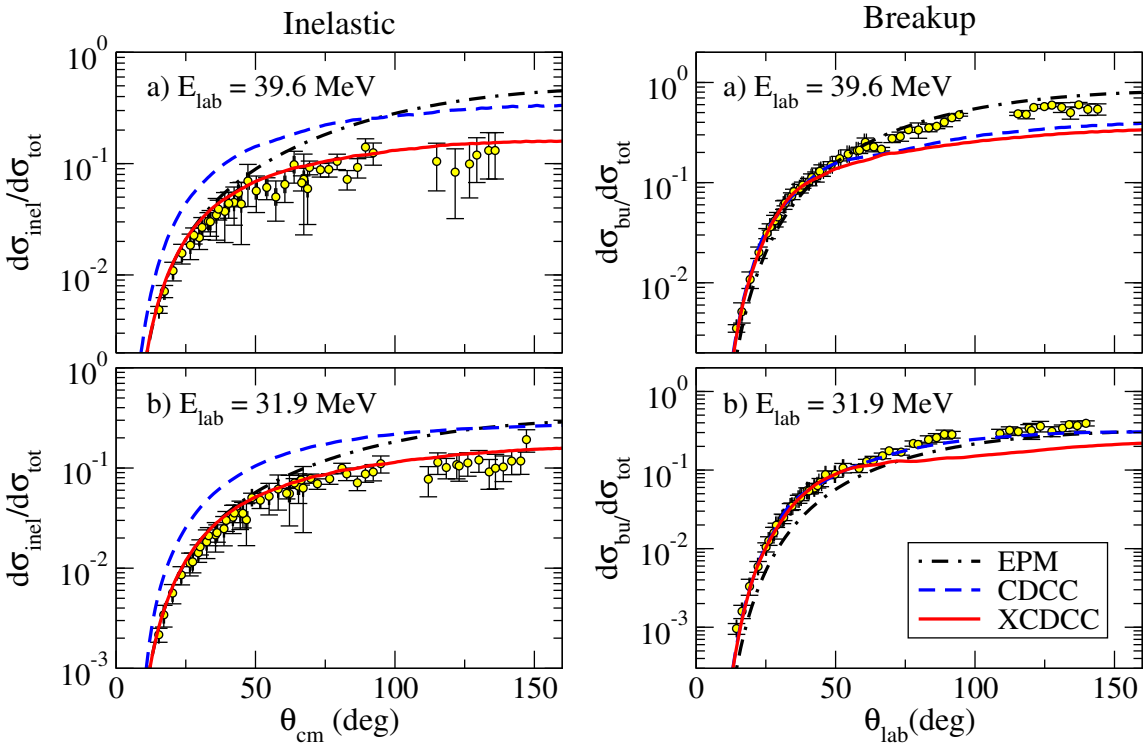

Figure 3: The experimental differential inelastic and break-up probabilities for ^{11}Be + ^{197}Au at energies of E_{lab} = 39.6 MeV (top) (*a*) and 31.9 MeV (*b*) (bottom) are compared with different calculations. The differential inelastic probability is shown on the left hand side of the figure in centre of mass frame. The differential break-up probability is shown in the laboratory frame on the right hand side. The EPM calculation succeeds (slightly overestimates within the error bars) in reproducing the inelastic channel at forward angles and underestimate the break-up channel mainly for energies below the barrier. CDCC overestimates the data as the calculated inelastic probabilities are a factor of 2 larger than the experimental values. It reproduces the break-up data at forward angles where the process is dominated by the Coulomb interaction. XCDCC reproduces well the inelastic channel at both energies for the full angular range and the break-up in the region where the process is dominated by the Coulomb interaction.

included in the description of the structure as well as in its interaction with the target. The XCDCC takes into account both the halo and core degrees of freedom.

Convergence of the studied observables for the CDCC and XCDCC calculations required a very large model space with $J^{\pi} \leq 15/2^{\pm}$ and an excitation energy up to 12 MeV for the total momentum and excitation energy of ^{11}Be , and narrow energy bins of $\sim$ 140 keV at excitation energies close to the threshold. Both models yield similar total $B(E1)$ as both have similar root mean square radii for the halo neutron of the ^{11}Be ground state, although the particle-rotor model gives slightly large $B(E1)$ to the continuum than the single particle used in CDCC but both are compatible with the experimental value of [14]. For the $B(E1)$ between bound states the results are reversed, showing the single particle model an important overestimation that will affect the inelastic cross section as shown later.

Fig. 2 shows ^{11}Be + ^{197}Au elastic differential cross sections divided by Rutherford at 39.7 MeV (top) and 31.9 MeV (bottom) laboratory energies. The first relevant observation is that, even at energies below the barrier, there is a significant deviation of the elastic channel from the one expected in well bound nuclei, even at very forward angles (corresponding to very distant trajectories). This drastic change in the elastic cross section is a consequence of the halo structure, and a the signature of dipole polarizability [16]. The data were first compared with an optical model calculation using as starting parameters those obtained from the fit of the ^{10}Be + ^{208}Pb elastic data at similar energies [19]. In order to reproduce the experimental elastic differential cross section the diffuseness parameters have to be increased by large factors both for the real and mainly in the imaginary part of the potential. Further details are given in [17]. These results indicate the sensitivity to long distances, the importance of the long range coupling and the dominance of Coulomb interaction in the process. The elastic data are compared with the large scale CDCC and XCDCC calculations. Interestingly enough, the elastic and inelastic data, see Fig. 3, are not reproduced by the standard CDCC method,

Table 2 shows the total reaction cross section and separate angle-integrated reaction, inelastic, break-up and absorption cross sections. The latter accounts for the channels not explicitly included in the CDCC model space, but taken effectively into account by means of the imaginary potentials, such as target excitation, neutron transfer and fusion (complete and incomplete). First one should notice that the reaction cross section increases with the energy of the projectile as expected when going from energies below the Coulomb barrier to energies around the Coulomb barrier. Furthermore the reaction cross section is much larger for the CDCC calculation than for the XCDCC one. This is due mainly to the large inelastic scattering channel that contributes 58 % and 55 % at the ^{11}Be + ^{197}Au at 31.9 and 39.6 MeV energies, respectively. As shown in Fig. 3, the CDCC inelastic cross section overestimates the inelastic data at both energies in the full angular range, while the XCDCC calculation follows the differential inelastic probability distribution well in both cases. We can trace back the origin of this result to the fact that the SP model overestimates the experimental $B(E1)$ between bound states by a factor of two. It is also relevant to mention that the relative role played by the break-up and absorption channels is larger in the XCDCC calculation compare to the CDCC one being the absorption channel the one that grows more with the energy. In all cases the inelastic and break-up dominate the reaction cross section. Considering that the break-up channels are very similar in both CDCC and XDCC calculations and the elastic and inelastic are respectively under- and over-estimated in the CDCC calculation, one can expect that the CDCC calculation will

reproduce well the quasielastic data. This was the case for ^{11}Be + ^{64}Zn [26]. By comparing our differential quasielastic cross section with the CDCC calculation we recovered, as shown in Fig. 2, the validity of the CDCC calculation. We dare to say that only a very complete experiment can do an stringent test of the model.

Fig. 3 shows the angular distribution of ^{11}Be + ^{197}Au reaction channels at 39.6 MeV(top) and 31.6 MeV (bottom). On the left hand side the inelastic probability is shown. It is defined for each angular bin as the number of inelastic events selected by coincidence of the quasielastic events with the 320 keV γ-line divided by the efficiency of the TIGRESS array at this γ-ray energy and divided by the total number of scattered events. The angular distribution is given in the centre of mass frame. On the right hand side of Fig. 3 the break-up probability, defined as the ratio of break-up events divided by the total number of scattered events, is shown. The angular distribution is given in this case in the laboratory framework.

Semiclassical first-order calculations reproduce the inelastic scattering at forward angles up to the grazing angle where the main process is Coulomb ecitation. The calculation reproduces also the break-up data at forward angles where the process is clearly direct for the energy around the Coulomb barrier, but under predicts the inelastic probability distribution of ^{11}Be + ^{197}Au at 31.6 MeV in the full angular range. The CDCC has been successfully used to describe the scattering with high-Z targets of other halo nuclei such as ^{6}He and ^{11}Li [3, 4, 5, 6, 7], and it is able to describe well the quasielastic scattering data of ^{11}Be with intermediate-Z targets like Zn [26] and the quasielastic scattering. In our case the CDCC calculation reproduces the breakup data rather well. However, the elastic and inelastic channels are in clear disagreement with the data (Figs. 2 and 3). The calculated inelastic probabilities are a factor of 2 larger than the experimental values, see Table 2. This is expected, since the assumed SP model gives $B(E1)$= 0.26 e^{2}fm^2 for the transition between the 1/2$^+$ ground state and the 1/2$^-$ bound excited states, which is twice as large as the experimental value. The CDCC calculation reproduces the quasielastic data well. The XCDCC give a very good reproduction of the experimental data in all channels.

.

4. Summary

The scattering of ^{11}Be + ^{197}Au has been studied with efficient gamma-particle coincidences, obtained with high granularity, and good energy resolution. This optimal device has allowed to extract the differential elastic, inelastic and break-up cross sections measured in a wide angular range at energies below (31.9 MeV) and around (39.6 MeV) the Coulomb barrier ($V_b \approx 40$ MeV). This is the first time that the three major channels have been separated in this energy regime.

The inelastic and break-up channels are important even at energies well below the Coulomb barrier. Calculations including all processes and the continuum are required. Semiclassical first-order calculations reproduce the inelastic scattering at forward angles, while they underestimate the break-up along the full angular range to a larger extent at energies well below the Coulomb barrier. This indicates that the inelastic scattering is mainly a one-step Coulomb process whereas the break-up has important contributions beyond direct Coulomb break-up. CDCC fails to reproduce the elastic and inelastic channels separately while it is able to reproduce the quasielastic one. XCDCC

calculations are necessary to explain simultaneously break-up and inelastic scattering data. The results show that the reaction mechanism is sensible to subtle structure features as core deformation.

For first time, state-of-art couple channel calculations describe the complex interplay between the halo and the core degrees of freedom (XCDCC). This new calculation has proven to be essential to describe the data consistently. This theoretical calculation that reproduces consistently the three channels validate the $B(E1)$ distribution of ref. [14]. Further details are provided elsewhere [27].

References

[1] P. G. Hansen and B. Jonson, *Europhys. Lett.* **4** (1987) 409.

[2] I. Tanihata et al., *Phys. Rev. Lett.* **55** (1985) 2676.

[3] D. Escrig et al., *Nuc. Phys. A* **792** (2007) 2.

[4] A.M. Sánchez-Benítez et al., *Nuc. Phys. A* **803** (2008) 30.

[5] L. Acosta et al., *Phys. Rev. C* **84** (2011) 044604.

[6] M.A. Cubero et al., *Phys. Rev. Lett.* **109** (2012) 262701.

[7] J.P. Fernández-García et al., *Phys. Rev. Lett.* **110** (2013) 142701.

[8] T. Nakamura et al., *Phys. Rev. Lett.* **96** (2006) 252502.

[9] P. G. Hansen, *Nuc. Phys. A* **682** (2001) 310c.

[10] D. Millener et al., *Phys. Rev. C* **28** (1983) 497.

[11] E. Kwan et al., *Phys. Lett. B* **732** (2014) 210.

[12] T. Nakamura et al., *Phys. Lett. B* **331** (1994) 296.

[13] R. Palit et al., *Phys. Rev. C* **68** (2003) 034318.

[14] N. Fukuda et al., *Phys. Rev. C* **70** (2004) 054606.

[15] G. Ball et al., *Nuc. Phys. A* **787** (2007) 118c.

[16] M. V. Andrés and J. Gómez-Camacho, *Phys. Rev. Lett.* **82** (1999) 1387.

[17] V. Pesudo et al., *Phys. Rev. C, in preparation*.

[18] K. Alder and A. Winter, *Electromagnetic Excitation* (North Holland, Amsterdam, 1975).

[19] J. J. Kolata et al., *Phys. Rev. C* **69** (2004) 047601.

[20] A. J. Koning and J. P. Delaroche, *Nucl. Phys. A* **713** (2003) 231.

[21] P. Capel, G. Goldstein and D. Baye, *Phys. Rev. C* **70** (2004) 064605.

[22] T. Tarutina, L. Chamon and M. Hussein, *Phys. Rev. C* **67** (2003) 044605.

[23] F. Nunes et al., *Nuc. Phys. A* **609** (1996) 43.

[24] N. Summers, F. Nunes and I. Thompson, *Phys. Rev. C* **73** (2006) 031603.

[25] R de Diego et al., *Phys. Rev. C* **89** (2014) 064609.

[26] A. Di Pietro et al., *Phys. Rev. C* **85** (2012) 054607.

[27] V. Pesudo et al., *Phys. Rev. Lett., submitted*.